TUM-HEP-501/03

Neutrino Masses, Oscillations, and Tests with Future Superbeams and a Neutrino Factory[†]

M. Lindner

Abstract:

Future long baseline neutrino oscillation (LBL) setups are discussed and the remarkable potential for very precise measurements of mass splittings, mixing angles, MSW effects, the sign of Δm^2 and leptonic CP violation is shown. Furthermore we discuss the sensitivity improvements which can be obatined by combining the planned JHF-Superkamiokande and the proposed NuMI off-axis experiment.

1 Introduction

Atmospheric neutrino oscillations are by now well established, since there exists even some sensitivity to the characteristic L/E dependence of oscillations [1]. The length scale L_{atm} of atmospheric oscillations is for $\Delta m^2_{31} \simeq 3{\cdot}10^{-3}\,\mathrm{eV}$, and for neutrino energies of $E_\nu \simeq 10\,\mathrm{GeV}$, about $L_{atm} \simeq O(2000)$ km. This are distances and energies which can also be probed with neutrino beams which are sent from one point on the Earth to another. Flavour transitions [2, 3] of solar neutrinos are also well established and oscillation is under all alternatives the most plausible explanation. The favored LMA solution for the mass splittings and mixings [4] has been confirmed for reactor anti-neutrinos by by the KamLAND experiment [5]. The CHOOZ reactor experiment [6] provides moreover currently the most stringent upper bound for the sub-leading U_{e3} mixing matrix element. The global pattern of neutrino oscillation parameters is therefore quite well known and one may ask how precise future long baseline experiments (LBL) will ultimately be able to measure the mass splittings and mixings and what can be learned from such precise measurements.

A promising first generation of LBL experiments exists already (KEK) or is under construction (MINOS, CNGS). We discuss [7] here the remarkable potential of experiments beyond this first generation. We compare therefore different potential setups individually, as well as in combination. The remarkable precision which can be obtained tests the three-flavouredness of oscillations. θ_{13} can be measured much better than today and it will be possible to study MSW matter effects and to extract $sign(\Delta m^2_{31})$. For the now confirmed LMA case, it will also be possible to measure leptonic CP violation [8]. Such precise neutrino masses, mixings and CP phases constitutes extremely valuable flavour information, since unlike for quarks, they are not obscured by hadronic uncertainties. These

[†]To appear in the proccedings of the conference "Neutrinos and Implications for Physics Beyond the Standard Model", Oct. 11-13, 2002, Stony Brook, USA

parameters can be evolved with the renormalization group to the GUT scale to be compared with models for neutrino masses and mixings. Leptonic CP violation is moreover related to leptogenesis, the currently most plausible mechanism for the generation of the baryon asymmetry of the universe. LBL experiments offer therefore in a unique way access to extremely interesting and valuable physics parameters.

2 Beams and Detectors

LBL experiments have the advantage that both source and detector can be kept under precise conditions. This includes amongst others for the source a precise knowledge of the mean neutrino energy E_ν, the neutrino flux and spectrum, as well as the flavour composition and contamination of the beam. Another important aspect is whether neutrino and anti-neutrino data can be obtained symmetrically such that systematical uncertainties cancel. Precise measurements require also a sufficient luminosity and a detector such that enough statistics can be obtained. On the detector side one must include further issues, like the detection threshold function, energy calibration, resolution, particle identification capabilities (flavour, charge, event reconstruction, backgrounds). Another source of uncertainty in the detection process is the knowledge of neutrino cross-sections, especially at low energies [9]. Source and detector combinations of a future LBL experiment are furthermore constraint by the available technology.

The first type of considered sources are conventional neutrino and anti-neutrino beams, where an intense proton beam is directed onto a massive target producing mostly pions and some K mesons, which are captured by an optical system of magnets in order to obtain a beam. The pions (and K mesons) decay in a decay pipe, yielding essentially a muon neutrino beam which can undergo oscillations as shown in fig. 1. Most interesting are the $\nu_\mu \to \nu_\mu$ disappearance channel and the $\nu_\mu \to \nu_e$ appearance channels.

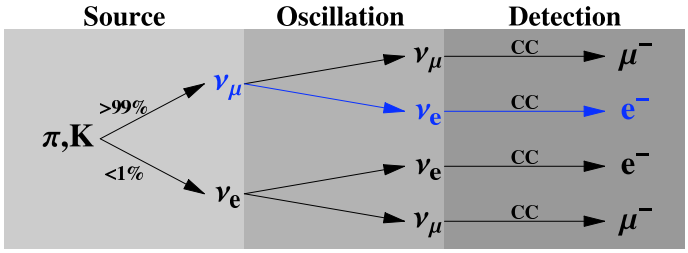

Figure 1: *Neutrino production, oscillation and detection via charged current interactions for conventional beams. The $\nu_\mu \to \nu_\mu$ disappearance and $\nu_\mu \to \nu_e$ appearance channels are most interesting, but the ν_e beam contamination at the level of $< 1\%$ limits the ability to determine the $\nu_\mu \to \nu_e$ appearance oscillation, since it produces also electrons.*

The neutrino beam is, however, contaminated by approximately 0.5% electron neutrinos, which also produce electron reactions in the disappearance channel, limiting thus the precision in the extraction of $\nu_\mu \to \nu_e$ oscillation parameters. The energy spectrum of the muon beam can be controlled over a wide range: it depends on the incident proton energy, the optical system, and the precise direction of the beam axis compared to the direction of

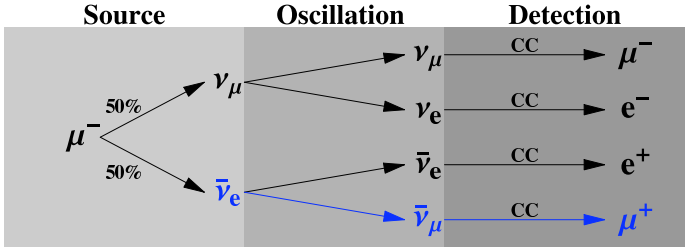

Figure 2: *Neutrino production, oscillation and detection via charged current interactions for neutrino factories.* $\overline{\nu}_e$ *and* ν_μ *are produced in equal numbers from* μ*-decays and can undergo different oscillations. The* $\nu_\mu \to \nu_\mu$ *and* $\overline{\nu}_e \to \overline{\nu}_\mu$ *channels are most interesting for detectors with* μ *identification. Note, however, that excellent charge identification capabilities are required to separate "wrong sign muons" and "right sign muons".*

the detector. It is possible to produce broad band high energy beams, such as the CNGS beam [10, 11], or narrow band lower energy beams, such as in some configurations of the NuMI beam [12]. Reversing the electrical current in the lens system results in an anti-neutrino beam. The neutrino and anti-neutrino beams have significant differences such that errors do not cancel systematically in ratios or differences. The neutrino and anti-neutrino beams must therefore more or less be considered as independent sources with different systematical errors.

"Superbeams" use the same techniques for producing neutrino beams, but at much larger luminosities [10, 11, 12, 13]. Superbeams are thus a technological extrapolation of conventional beams, with a proton beam intensity close to the mechanical stability limit of the target at a typical thermal power of 0.7 MW to 4 MW. The much higher neutrino luminosity allows the use of the decay kinematics of pions to produce so–called "off–axis beams", where the detector is located some degrees off the beam axis. This reduces the neutrino flux and the average neutrino energy, but leads to a more mono-energetic beam and a significant suppression of the electron neutrino contamination. Several off–axis superbeams with energies of about 1 GeV to 2 GeV have been proposed in Japan [14, 15], America [16], and Europe [17, 18].

The most sensitive neutrino oscillation channel for sub-leading oscillation parameters is the $\nu_\mu \to \nu_e$ appearance transition. Therefore the detector should have excellent electron and muon charged current identification capabilities. In addition, an efficient rejection of neutral current events is required, because the neutral current interaction mode is flavor blind. With low statistics, the magnitude of the contamination itself limits the sensitivity to the $\nu_\mu \to \nu_e$ transition severely, while the insufficient knowledge of its magnitude constrains the sensitivity for high statistics. A near detector allows a substantial reduction of the background uncertainties [14, 19] and plays a crucial role in controlling other systematical errors, such as the flux normalization, the spectral shape of the beam, and the neutrino cross section at low energies. At energies of about 1 GeV, the dominant charge current interaction mode is quasi–elastic scattering, which suggests that water Cherenkov detectors are the optimal type of detector. At these energies, a baseline of about 300 km would be optimal to measure at the first maximum of the oscillation. At about 2 GeV, there is already a considerable contribution of inelastic scattering to the charged current interactions, which means that it would be useful to measure the energy of the hadronic part of the cross

section. This favors low–Z hadron calorimeters, which also have a factor of ten better neutral current rejection capability compared to water Cherenkov detectors [16]. In this case, the optimum baseline is around 600 km. The matter effects are expected to be small for these experiments for two reasons. First of all, an energy of about 1 GeV to 2 GeV is small compared to the MSW resonance energy of approximately 13 GeV in the upper mantle of the Earth. The second reason is that the baseline is too short to produce significant matter effects.

The second type of beam considered are so-called neutrino factories, where muons are stored in the long straight sections of a storage ring. The decaying muons produce muon and electron anti-neutrinos in equal numbers [20]. The muons are produced by pion decays, where the pions are produced by the same technique as for superbeams. After being collected, they have to be cooled and re-accelerated very quickly. The spectrum and flavor content of the beam are completely characterized by the muon decay and are therefore very precisely known [21]. The only adjustable parameter is the muon energy E_μ, which is usually considered in the range from 20 GeV to 50 GeV. It is possible to produce and store anti-muons in order to obtain a CP conjugated beam and the symmetric operation of both beams leads to the cancellation or significant reduction of errors and systematical uncertainties. Unless stated differently, we discuss the neutrino beam including implicitly the CP conjugate channel.

The decay of the muons and the relevant oscillation channels are shown in fig. 2. Amongst all flavors and interaction types, muon charged current events are the easiest to detect. The appearance channel with the best sensitivity is thus the $\overline{\nu}_e \to \overline{\nu}_\mu$ transition, which produces so called "wrong sign muons". Therefore, a detector must be able to very reliably identify the charge of a muon in order to distinguish wrong sign muons in the appearance channel from the higher rate of same sign muons in the disappearance channels. The dominant charge current interaction in the multi– GeV range is deep–inelastic scattering, making a good energy resolution for the hadronic energy deposition necessary. Magnetized iron calorimeters are thus the favored choice for neutrino factory detectors. In order to achieve the required muon charge separation, it is necessary to impose a minimum muon energy cut at approximately [22, 23] at 4 GeV. This leads to a significant loss of neutrino events in the range of about 4 GeV to 20 GeV, which means that a high muon energy of $E_\mu = 50$ GeV is desirable. The first oscillation maximum lies then at approximately 3 000 km. Matter effects are sizable at this baseline and energy, and the limited knowledge of the Earth's matter density profile becomes an additional source of errors.

3 Simulations of specific LBL Setups

The results shown in this article were obtained in a numerical simulation of the setups including exact oscillation probabilities in matter. There are numerous experimental and phenomenological details which have to be included in such an analysis. Their descriptin goes beyond the scope of this article, but all details are described in the literature [7]. A qualitative analytic understanding of the results can be obtained by expanding the oscillation probaibilities in small quantities [24, 25, 26]. The presented results can thus be understood qualitatively with analytic equations [7].

Table 1: *The considered combinations of beams and detectors and their acronyms.*

acronym	detector	L	L/E_{peak}
JHF-SK	water Cherenkov	295	378
NuMI	low-Z	735	337
NuFact-I	10 kt mag. iron	3000	90
JHF-HK	water Cherenkov	735	295
NuFact-II	40 kt mag. iron	3000	90

We consider different beams and detectors which allow interesting combinations as listed in Table 1. JHF-SK is the planned combination of the existing SuperKamiokande detector and the JHF beam, while JHF-HK is the combination of an upgraded JHF beam with the proposed HyperKamiokande detector. With typical parameters, JHF-HK is altogether about 95 times more integrated luminosity than JHF-SK, and we assume that it operates partly with the anti-neutrino beam. Water Cherenkov detectors are ideal for the JHF beam, since charged current quasi elastic scattering is dominating. A low-Z calorimeter is proposed for the NuMI off-axis beam, which is better here, since the energy is higher and there is already a considerable contribution of inelastic charged current interactions. NuFact-I is an initial neutrino factory, while NuFact-II is a fully developed machine, with 42 times the luminosity of NuFact-I [14, 16, 22]. Deep inelastic scattering dominates for these even higher energies and magnetized iron detectors are therefore considered in combination with neutrino factories.

Our study [7] includes all relevant aspects and we find the following results. There is excellent precision for the leading oscillation parameters Δm^2_{31} and $\sin^2 2\theta_{23}$, which will not be further discussed here. The more interesting sensitivity to the sub-leading parameter $\sin^2 2\theta_{13}$ depends on what will be found for Δm^2_{31} and Δm^2_{21}. Assuming that the leading parameters are measured to be $\Delta m^2_{31} = 3 \cdot 10^{-3}\,\text{eV}^2$, $\sin^2 2\theta_{23} = 0.8$ and that KamLAND measures the solar parameters at the current best fit point of the LMA region, *i.e.* $\Delta m^2_{21} = 6{\cdot}10^{-5}\,\text{eV}^2$ and $\sin 2\theta_{12} = 0.91$, we can make a comparison of the $\sin^2 2\theta_{13}$ sensitivity limit for the different setups. The result is shown in fig. 3. The individual contributions of different sources of uncertainties are shown for every experiment. The left edge of every band of fig. 3 corresponds to the sensitivity limit which would be obtained purely on statistical grounds. This limit is successively reduced by adding the systematical uncertainties of each experiment, the correlational errors and finally the degeneracy errors. The right edge of each band constitutes the final error for the experiment under consideration. It is interesting to see how the errors of the different setups are composed. There are different sensitivity reductions due to systematical errors, correlations and degeneracies. The largest sensitivity loss due to correlations and degeneracies occurs for NuFact-II.

Another challenge of future LBL experiments is to measure $sign(\Delta m^2_{31})$ via matter effects and the sensitivity which can be obtained for the setups under discussion is shown in fig. 4. Taking all correlational and degeneracy errors into account we can see that it is very hard to determine $sign(\Delta m^2_{31})$ with the considered superbeam setups. The main problem is the degeneracy with δ, which allows always the reversed $sign(\Delta m^2_{31})$ for another CP phase. Note, however, that the situation can in principle be improved if different superbeam exper-

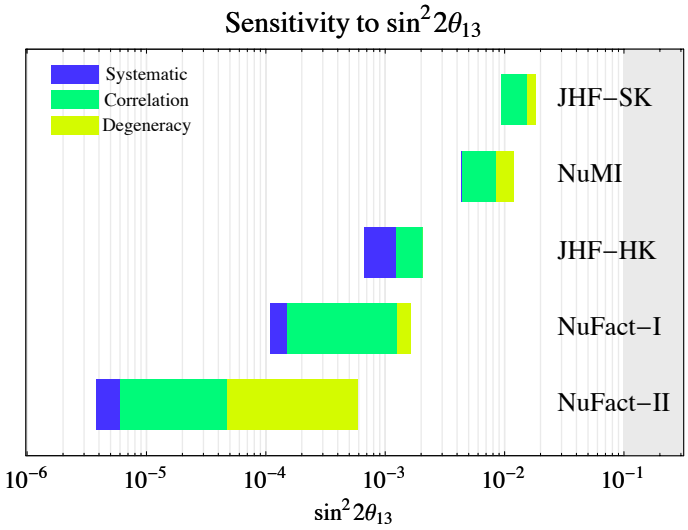

Figure 3: *The* $\sin^2 2\theta_{13}$ *sensitivity for the setups defined in section 3 at 90% CL for* $\Delta m^2_{31} = 3 \cdot 10^{-3}\,\mathrm{eV}^2$ *and* $\sin^2 2\theta_{23} = 0.8$*. The plot shows the deterioration of the sensitivity limits as the different error sources are successively switched on. The left edge of the bars is the sensitivity statistical limit. This limit gets reduced as systematical, correlational and degeneracy errors are switched on. The right edge is the final sensitivity limit [7].*

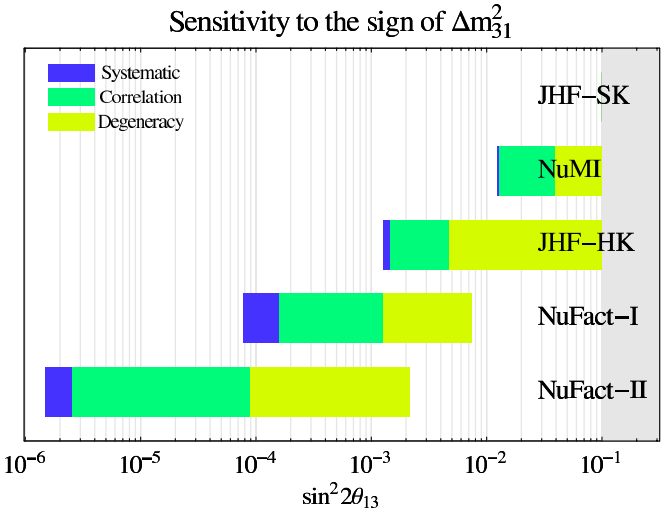

Figure 4: *The* $\sin^2 2\theta_{13}$ *sensitivity region to* $sign(\Delta m^2_{31})$ *for all considered setups as defined in section 3 at 90% CL for* $\Delta m^2_{31} = 3 \cdot 10^{-3}\,\mathrm{eV}^2$ *and* $\sin^2 2\theta_{23} = 0.8$*. The plot shows how the sensitivity limits become worse as the different error sources are successively switched on. The left edge of the bars is the sensitivity statistical limit. This limit gets reduced as systematical, correlational and degeneracy errors are switched on. The right edge is the final sensitivity limit [7].*

iments were combined such that this degeneracy error could be removed. Neutrino factories perform considerably better on $sign(\Delta m^2_{31})$, particularly for larger baselines. Combination strategies would again lead to further improvements.

Coherent forward scattering of neutrinos and the corresponding MSW matter effects are so far experimentally untested. It is therefore very important to realize that matter effects will not only be useful to extract $sign(\Delta m^2_{31})$, but that they allow also detailed tests of coherent forward scattering of neutrinos. This has been studied in detail [26, 27, 28, 29].

The Holy Grail of LBL experiments is the measurement of leptonic CP violation. The

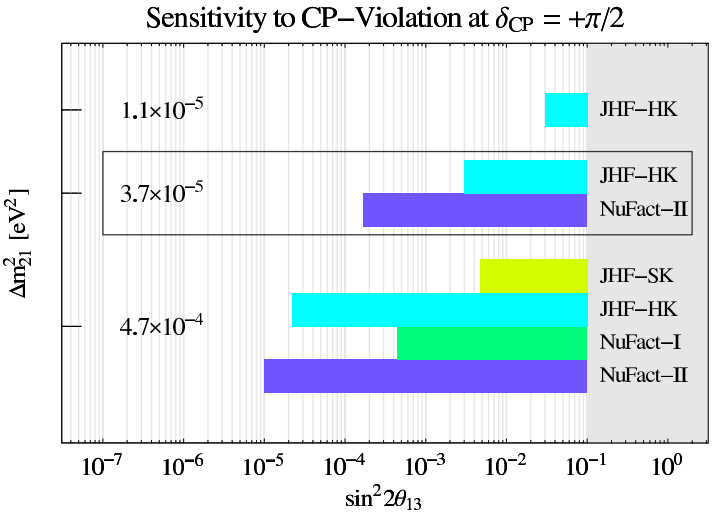

Figure 5: *The* $\sin^2 2\theta_{13}$ *sensitivity range for CP violation of the considered setups at 90% confidence level and for different* Δm^2_{21} *values. The upper row corresponds to the lower bound of* $\Delta m^2_{21} = 1.1 \times 10^{-5}\,\mathrm{eV}^2$*, the bottom row to the upper bound* $\Delta m^2_{21} = 4.7 \times 10^{-4}\,\mathrm{eV}^2$*, and the middle row to the best LMA fit,* $\Delta m^2_{21} = 3.7 \times 10^{-5}\,\mathrm{eV}^2$*. Cases which do not have CP sensitivity are omitted from this plot. The chosen parameters are* $\delta = +\pi/2$*,* $\Delta m^2_{31} = 3{\cdot}10^{-3}\,\mathrm{eV}^2$*,* $\sin^2 2\theta_{23} = 0.8$*, and a solar mixing angle corresponding to the current best fit in the LMA regime [7].*

$\sin^2 2\theta_{13}$ sensitivity range for measurable CP violation is shown in fig. 5 for $\delta = \pi/2$ for the different setups and for different values of Δm^2_{21}. It can be seen that measurements of CP violation are in principle feasible both with high luminosity superbeams as well as advanced neutrino factories. However, the sensitivity depends in a crucial way on Δm^2_{21}. For a low value $\Delta m^2_{21} = 1.1\ 10^{-5}\,\mathrm{eV}^2$, the sensitivity is almost completely lost, while the situation would be very promising for the largest considered value $\Delta m^2_{21} = 4.7\ 10^{-4}\,\mathrm{eV}^2$. For a measurement of leptonic CP violation it would therefore be extremely exciting and promising if KamLAND would find Δm^2_{21} on the high side of the LMA solution (the so-called HLMA case). The sensitivities shown in fig. 5 depend on the choice for δ. The value which was used here was $\delta = \pi/2$ and and the sensitivities become become worse for small CP phases close to zero or π.

4 Combining LBL Setups

We have compared so far the potential of individual LBL setups. If two LBL setups with similar strength are realized simultaneously then it becomes possible to combine the analysis of these two experiments, leading to improved statistics of a global fit. However,

if the two setups are planned correctly, then much more can be gained, since some of the correlations and degeneracies of individual experiments can be removed. This could, for example, already be relevant if both JHF-SK and NUMI were built. We analyzed therefore the potential of such a scenario [30]. We assume therefore for both experiments setups as given in the respective letters of intent. We allow, however, for modifications in the NuMI baseline and we allow for both experiments different options for neutrino and antineutrino running. The considered scenarios are listed in Table 2.

Table 2: *Overview of combined JHF-SK and NuMI scenarios. Listed are the fraction of neutrino and antineutrino running both for JHF-SK NuMI. The chosen baselines and the corresponding off-axis angles are shown in addition for the NuMI experiment. The last column contains the label which is used in the following figures to identify the scenarios. The label contains first the three digit baseline (in km), then the JHF and NuMI running modes, where ν, $\overline{\nu}$ and c stand for neutrino, antineutrino and mixed running mode, respectively.*

JHF-SK		NuMI				Scenario
ν	$\overline{\nu}$	ν	$\overline{\nu}$	L [km]	OA angle	Label
1	0	1	0	712	0.72°	712$\nu\nu$
1	0	1	0	890	0.72°	890$\nu\nu$
1	0	1	0	950	0.97°	950$\nu\nu$
2/8	6/8	2/7	5/7	712	0.72°	712cc
2/8	6/8	2/7	5/7	890	0.72°	890cc
2/8	6/8	2/7	5/7	950	0.97°	950cc
1	0	0	1	712	0.72°	712$\nu\overline{\nu}$
1	0	0	1	890	0.72°	890$\nu\overline{\nu}$
1	0	0	1	950	0.97°	950$\nu\overline{\nu}$
0	1	1	0	712	0.72°	712$\overline{\nu}\nu$
0	1	1	0	890	0.72°	890$\overline{\nu}\nu$
0	1	1	0	950	0.97°	950$\overline{\nu}\nu$

Fig. 6 shows the resulting limits for the $\sin^2 2\theta_{13}$ sensitivity for the various combined JHF-SK and NuMI setups. The statistical sensitivity limit (left edge of the bars) is in all cases reduced, but due to the reduction of correlations and degeneracies many of the setups perform in the end better than the individual setups after all sources of errors are included (right edge of the bars). The improvements are a result of the partial complementarity of the different baselines and polarities and in the end, any of the shown setups has a rather good performance in the $\sin^2 2\theta_{13}$ sensitivity. It should, however, not be forgotten that the uncertainties of the atmospheric and solar mass squared differences can affect this result much stronger than choosing the suboptimal solution. The sensitivity limits are shifted to higher values for larger values of Δm^2_{21} and to smaller values for smaller values of Δm^2_{21}. For $\Delta m^2_{21} \simeq 3 \cdot 10^{-4}\,\mathrm{eV}^2$ the CHOOZ bound would be reached, but this value is already ruled out by combining the recent KamLAND data with all other data [31].

The combination of the JHF-SK and NuMI experiments lead also to improvements in the sensitivity to leptonic CP violation. Fig. 7 shows the combined limits for the sensitivity to a maximal CP phase, *i.e.*, $\delta = \pm\pi/2$. The sensitivity limits for other CP phases are weaker

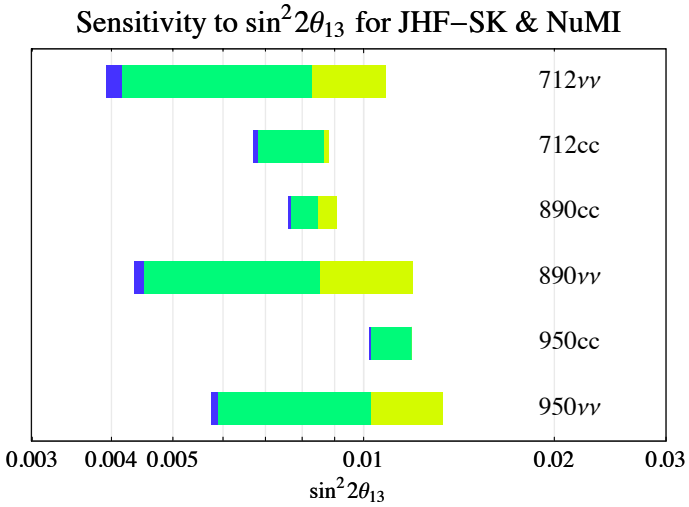

Figure 6: *The* $\sin^2 2\theta_{13}$ *sensitivities (90% CL) for different combinations of JHF-SK and NuMI. The labels indicate the NuMI baseline in km followed by two characters indication the running modes of JHF-SK (first character) and NuMI (second character) experiments for a selected set of the alternative options and the original combination (first bar). The labels are defined in Table 1. The left edges of the bars correspond to the sensitivity limits from statistics only. The right edges of the bars correspond to the real sensitivity limits after successively switching on systematical, correlational, and degeneracy errors.*

and the limit or the precision of the δ measurement depend thus on δ. However, we expect the qualitative behavior to be similar to the case of maximal CP violation.

Fig. 8 shows the combined limits for the sensitivity to the sign of Δm^2_{31} at the LMA best-fit point for the original setup and the best alternative setups. In this figure, the left edges of the bars correspond again to the purely statistical sensitivity limits. Successively switching on systematical, correlational, and degeneracy errors reduces the sensitivity limit to the final answer, which is the right edge. It is very difficult to define the difference between correlations and degeneracies in this case, and we fix therefore $\delta = 0$ at the border of the second and third bars. There is no sensitivity to the sign of Δm^2_{31} for the original setup, while there is sensitivity at longer baselines. Which of the two proposed alternative baselines performs better depends on the exact value of Δm^2_{21}. From a purely statistical point only, the 890 km option is much better.

Fig. 9 shows a superposition of the regions of sign of Δm^2_{31} and CP violation sensitivity in the $\sin^2 2\theta_{13}$-Δm^2_{21}-plane at the 90% confidence level for the 890$\nu\nu$ (sign of Δm^2_{31}) and 890cc (CP violation) setups as defined in Table 2. It can be seen that the initial stage experiments might have a good chance to see either maximal CP violation or the sign of Δm^2_{31}. A simultaneous measurement of both quantities is in general hard to achieve. The recent KamLAND results [5] favor now two subregions in the LMA region. The central values are [31] $\Delta m^2_{21} \simeq 7 \cdot 10^{-5}\,\mathrm{eV}^2$ (LMA-I) and $\Delta m^2_{21} \simeq 1.5 \cdot 10^{-4}\,\mathrm{eV}^2$ (LMA-II). Note that both cases have some chance to measure maximal CP violation. The LMA-I case would allow for the 890$\nu\nu$ setup to measure the sign of Δm^2_{31} down to $\sin^2 2\theta_{13} \simeq 0.05$. The LMA-II case would allow for the central value and the 890cc setup a chance to measure maximal CP violation down to $\sin^2 2\theta_{13} \simeq 0.02$. The optimal running strategy for the combination

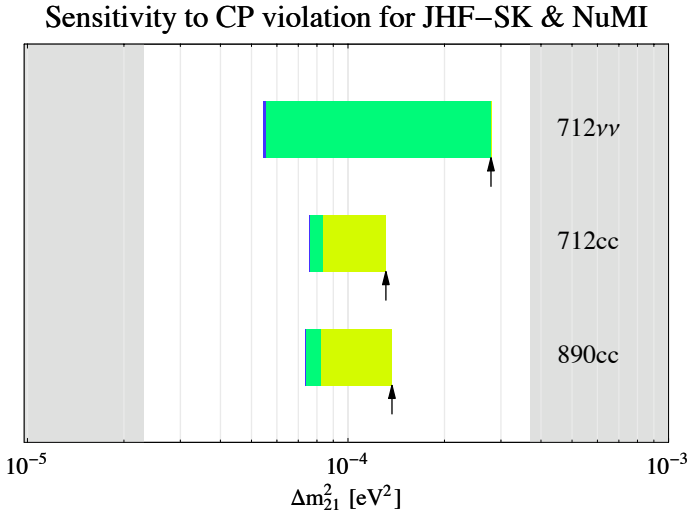

Figure 7: *Combined sensitivity limits to (maximal) CP violation in the Δm^2_{21} direction for fixed $\sin^2 2\theta_{13} = 0.03$ (90% CL, LMA values). The bars show the sensitivities of the combined JHF-SK and NuMI experiments for a selected set of options, where the labels are explained in Table 2. The first entry (712νν) corresponds to the setup as proposed in the LOIs. It can clearly be seen that the other two options with an increased baseline and a mixed running mode perform better. The left edges of the bars correspond again to the sensitivity limits from statistics only. The right edges of the bars correspond to the final sensitivity limits once systematics, correlations, and degeneracies are successively included. The gray area marks the LMA region.*

of JHF-SK and NuMI depends therefore crucially on the forthcoming improvements of the KamLAND data.

5 Conclusions

We discussed future long baseline neutrino oscillation experiments, which could be realized in stages and where every level leads to new results and serves at the same time as training ground for the next level. We showed that the individual experiments have a remarkable potential to measure neutrino oscillation parameters very precisely. We also showed that the combination of the JHF-SK and NuMI setups could do much better than any one of the experiments and it may in this way become possible to see CP violation or to measure the sign of Δm^2_{31} via matter effects. Long baseline neutrino oscillation experiments have altogether impressive potential to measure oscillation parameters very precisely. Such precise measurements of neutrino mass splittings and mixings would be extremely valuable, since unlike in the quark sector, the parameters do not have hadronic uncertainties. These parameters can be evolved with the renormalization group equations for the relevant dimension five operator for neutrino masses and mixings [32, 33, 34, 35] to the GUT scale, where they can be compared with models for neutrino masses. This could lead to interesting insights into the flavour problem. It is, for example, possible to explain in this way the deviation of the solar mixing angle from $\pi/4$ via quantum corrections to bi-maximality at the GUT scale [36]. The measurement of leptonic CP violation is by itself very interesting,

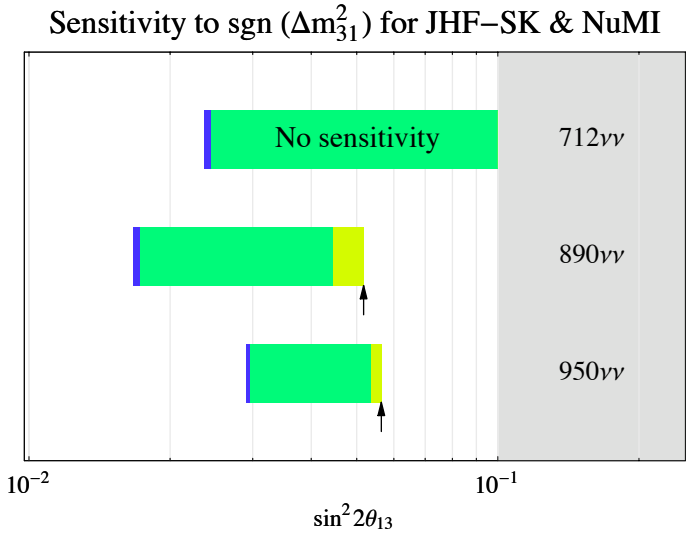

Figure 8: *Sensitivity limits for the sign of Δm^2_{31} in the $\sin^2 2\theta_{13}$ direction (90% CL, LMA values) for different combinations of JHF-SK and NuMI experiments. The first entry (712$\nu\nu$) corresponds to the setup as proposed in the LOIs. Other options with mixed running mode or longer baseline perform considerably better (labels as explained in Table 2). The left edges of the bars correspond to the statistical sensitivity limits. The right edges of the bars correspond to the real sensitivity limits after systematical, correlational, and degeneracy errors are successively switched on.*

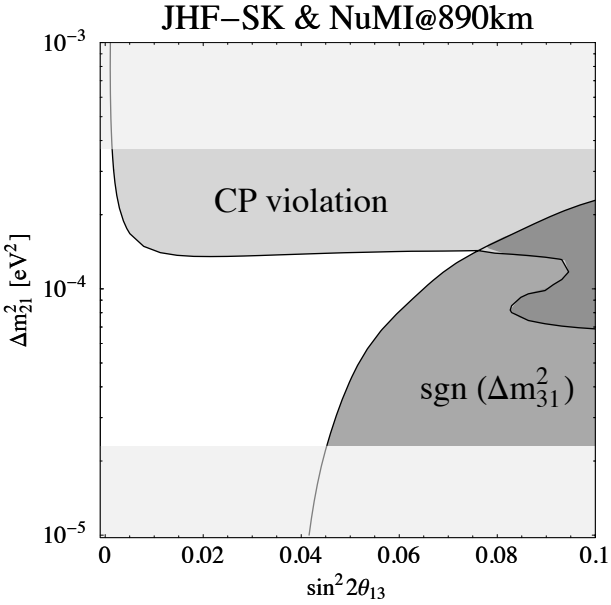

Figure 9: *The regions of sign of Δm^2_{31} and maximal CP violation sensitivity for the combined JHF-SK and NuMI experiments in the $\sin^2 2\theta_{13}$-Δm^2_{21}-plane (90% CL, LMA values). Shown are for the sign of Δm^2_{31} the 890$\nu\nu$ setup (neutrino running only) and for CP violation the 890cc setup (combined neutrino-antineutrino running). The LMA excluded region is shown in light gray.*

but it becomes even more interesting in models where it is connected to leptogenesis, the currently best explanation for the baryon asymmetry of the universe. This illustrates how important and promising future long baseline measurements are.

Acknowledgements: This work was supported by the "Sonderforschungsbereich 375-95 für Astro-Teilchenphysik" der Deutschen Forschungsgemeinschaft.

References

[1] T. Toshito (SuperKamiokande Collab.), hep-ex/0105023.

[2] Q. R. Ahmad *et al.* (SNO Collab.), Phys. Rev. Lett. **89**, 011301 (2002).

[3] Q. R. Ahmad *et al.* (SNO Collab.), Phys. Rev. Lett. **89**, 011302 (2002).

[4] See e.g. P. C. de Holanda and A. Yu. Smirnov, hep-ph/0205241.

[5] K. Eguchi *et al.*, [KamLAND Collaboration], hep-ex/0212021, Phys. Rev. Lett. **90** (2003) 021802.

[6] M. Apollonio *et al.* (Chooz Collab.), Phys. Lett. **B466**, 415 (1999).

[7] P. Huber, M. Lindner and W. Winter, hep-ph/0204352.

[8] K. Dick, M. Freund, M. Lindner, A. Romanino, Nucl. Phys. B **562** (1999) 29.

[9] E.A. Paschos, hep-ph/0204138.

[10] G. Acquistapace *et al.* (CNGS Collab.) CERN-98-02.

[11] R. Baldy *et al.* (CNGS Collab.) CERN-SL-99-034-DI.

[12] J. Hylen *et al.* (NuMI Collab.) FERMILAB-TM-2018.

[13] K. Nakamura (K2K Collab.), Nucl. Phys. **A663**, 795 (2000).

[14] Y. Itow *et al.*, hep-ex/0106019.

[15] M. Aoki, hep-ph/0204008.

[16] A. Para and M. Szleper, hep-ex/0110032.

[17] See e.g. J.J. Gomez-Cadenas *et al.*, hep-ph/0105297.

[18] F.Dydak, Rep., CERN (2002), http://home.cern.ch/dydak/oscexp.ps.

[19] M. Szleper and A. Para, hep-ex/0110001.

[20] S. Geer, Phys. Rev. **D57**, 6989 (1998).

[21] Particle Data Group, D.E. Groom *et al.*, Eur.Phys.J. C **15**, 1 (2000).

[22] A. Blondel *et al.*, Nucl. Instrum. Meth. **A451**, 102 (2000).

[23] C. Albright *et al.*, hep-ex/0008064, and references therein.

[24] A. Cervera *et al.*, Nucl. Phys. **B579**, 17 (2000).

[25] M. Freund, Phys. Rev. **D64**, 053003 (2001).

[26] M. Freund, P. Huber, and M. Lindner, Nucl. Phys. **B615**, 331 (2001).

[27] M. Freund, M. Lindner, S. T. Petcov and A. Romanino, Nucl. Phys. **B578**, 27 (2000).

[28] M. Freund, P. Huber, and M. Lindner, Nucl. Phys. **B585**, 105 (2000).

[29] M. Freund, M. Lindner, S.T. Petcov and A. Romanino, Nucl. Instrum. Meth. A **451**, 18 (2000).

[30] P. Huber, M. Lindner, and W. Winter, hep-ph/0211300, to appear in Nucl. Phys. B.

[31] See e.g. M. Maltoni, T. Schwetz and J. W. Valle, hep-ph/0212129.

[32] K. S. Babu, C. N. Leung and J. Pantaleone, hep-ph/9309223, Phys. Lett. **B319** (1993), 191.

[33] P.H. Chankowski and Z. Pluciennik, hep-ph/9306333, Phys. Lett. **B316** (1993), 312.

[34] S. Antusch, M. Drees, J. Kersten, M. Lindner and M. Ratz, hep-ph/0108005, Phys.Lett.B519 (2001) 238.

[35] S. Antusch, M. Drees, J. Kersten, M. Lindner and M. Ratz, hep-ph/0110366, Phys. Lett. B525 (2002) 130.

[36] S. Antusch, J. Kersten, M. Lindner and M. Ratz, hep-ph/0206078, Phys.Lett. B544 (2002) 1.